Nanoscale

PAPER

View Article Online
View Journal | View Issue

Cite this: *Nanoscale*, 2020, **12**, 4586

Wideband saturable absorption in metal–organic frameworks (MOFs) for mode-locking Er- and Tm-doped fiber lasers

Qian Zhang,†[a] Xiantao Jiang, †[b] Meng Zhang, *[a] Xinxin Jin,[a] Han Zhang *[c] and Zheng Zheng[a,d]

Received 2nd November 2019,
Accepted 15th January 2020

DOI: 10.1039/c9nr09330c

rsc.li/nanoscale

We fabricate a metal–organic framework (MOF) saturable absorber (SA) based on a microfiber. Nonlinear optical absorption of the MOF SA is characterized systematically. The modulation depth is found to be 6.57% and 14.25% at 1.5 and 2 μm spectral ranges, respectively. We report ultrashort pulse generation in both Er- and Tm-doped fiber lasers by using the same microfiber-based MOF SA, operating at 384 fs and 1.3 ps pulse duration at 1563 nm and 1882 nm, respectively. To the best of our knowledge, this is the first report of a MOF-based fiber laser at near infrared spectral ranges. Our findings validate the applicability of MOFs as a broadband SA in ultrafast photonics.

1. Introduction

Two-dimensional (2D) nanomaterials have been extensively studied due to their outstanding optical and optoelectronic properties. Recently, originating from the demonstration of graphene as a saturable absorber (SA) for ultrafast pulse generation, there have been immense advancements in the field of photonics based on 2D materials.[1] 2D materials have ultrafast carrier dynamics, 2D planar structures, and the advantage of wideband absorption. They have been demonstrated for a wide range of photonic and optoelectronic applications, such as photo-detectors,[2] optical modulators[3] and optical saturable absorbers (SAs).[4] A bunch of 2D nanomaterials, *e.g.*, graphene,[5] semiconducting transition metal dichalcogenides (s-TMDs),[6] and black phosphorus (BP),[7] have appeared as a good platform for a variety of nonlinear photonic and optoelectronic applications due to their remarkable properties, including ultrafast carrier dynamics, wideband working wavelength,[8] and high optical nonlinear susceptibility.[9] While these nanomaterials have been successfully applied as wideband saturable absorbers for short pulse generation, they still have limitations. For instance, the zero band-gap structure limits the application of graphene,[10] and the intrinsic band-gaps of s-TMDs are in the visible/near infrared region, limiting their practical applications.[11–13] BP has been reported to possess strong nonlinear optical properties, but the stability of BP-based devices are generally poor under ambient conditions, which is not ideal for applications requiring long-term stability.[14,15] Recently, metal–organic frameworks (MOFs) have triggered growing interest due to their remarkable merits, including large surface area, nanometer-sized spaces, ordered reticular structures, band-gap tunability, and compatibility of water and organic solvents.[16] They also have outstanding conductivity, high elastic moduli, and excellent optical transparency and electric capacity. Above all, the band-gap of nickel–*p*-benzenedicarboxylic acid metal–organic frameworks (Ni-MOFs) could be conveniently varied by controlling the doping concentration of Ni ions. It has been shown that the band-gap of Ni-MOFs decreases when the doping of Ni ions increases, indicating their excellent potential as SAs for applications in a wide operation spectral region.[17,18] According to the Cambridge Structural Database,[19] due to the richness of the chemical variety of organic ligands, there are almost about 2000 different MOF structures in the MOF family. The wide-range tunability suggests that MOFs can be tuned for all kinds of promising applications. To date, MOFs have led to a lot of applications, including molecular magnets,[20] gas storage,[21] chemical sensing,[22] nonlinear optics,[23] drug delivery[24] and so on. Due to the outstanding characteristics of Ni-MOFs as SAs, they may break new ground for the Ni-MOF-based nonlinear applications in ultrafast photonics.

Herein, we investigate the Ni-MOF characteristics, and report for the first time ultrafast pulse generation in both

[a]*School of Electronic and Information Engineering, Beihang University, Beijing, 100191, China. E-mail: mengzhang10@buaa.edu.cn*
[b]*College of Chemistry and Enviromental Engineering, Shenzhen University, Shenzhen, 518060, China*
[c]*Shenzhen Engineering Laboratory of Phosphorene and Optoelectronics, Shenzhen University, 518060, China. E-mail: hzhang@szu.edu.cn*
[d]*Collaborative Innovation Center of Geospatial Technology, Wuhan, 430079, China*
†These authors contributed equally to this work.

Er- and Tm-doped fiber lasers by using a microfiber-based Ni-MOF SA, operating at 1563 nm and 1882 nm, respectively. These results indicate that Ni-MOFs could be developed as a promising SA for ultrafast pulse generation.

2. Synthesis and characterization of the Ni-MOF

2.1 Fabrication of the Ni-MOF

The solvothermal method is considered as an effective technique to fabricate the Ni-MOF.[25] Briefly, *p*-benzenedicarboxylic acid (PTA) is added into the mixed solution which contains *N*-dimethylformamide (DMF) and alcohol. Nickel ions are supplied with $Ni(NO_3)_2{\cdot}6H_2O$ and then mixed with deionized water. The resulting mixture is then put into an autoclave for the formation of the crystalline Ni-MOF. After the crystallization process, the solution is cooled to room temperature. The resulted precipitate is washed with DMF and alcohol. The dispersion is centrifuged and dried to obtain the Ni-MOF powder.

2.2 Characterization of the Ni-MOF

Fig. 1(a) shows clearly the 2D crystal structure of the Ni-MOF. The Ni-MOF powder shows a typical 2D layer morphology as presented in Fig. 1b. The atomic force microscopy (AFM) image is obtained to study the morphology of the prepared Ni-MOF. This image is shown in Fig. 1(c). Two colored lines (blue and green) have been marked for the Ni-MOF powder. Height-profiling of the marked nanosheet is shown in Fig. 1(e), revealing a thickness of 4.2 nm. The Raman spectrum of the prepared Ni-MOF is shown in Fig. 1(d). There are five Raman peaks which can be resolved under the excitation of a 532 nm laser. The peaks at 632 and 862 cm^{-1} correspond to the in-plane deformation modes of C–H; the other peaks at 1136, 1427 and 1609 cm^{-1} are associated with the out-of-plane deformation modes of the C–H groups in the organic ligands.[26–28] The five active Raman modes are associated with the vibrational fingerprints of the *p*-benzene ring.

The Ni-MOF SA powder is then dissolved in an isopropanol solution. We use a homemade machine to fabricate the microfiber. In the process of fabrication, a 1554 nm continuous wave laser source with 1 mW saturation power is transferred to the microfiber. The power meter monitors the power change in real time. The power loss is about 0.3 dB before deposition. The tapered area of the optical fiber with a width of ~10 μm is observed directly under a microscope. We performed the optical deposition method to fabricate the microfiber.[29] We used a 1550 nm ASE pump light source with 50 mW saturation power in the process of photo-deposition. After the action of

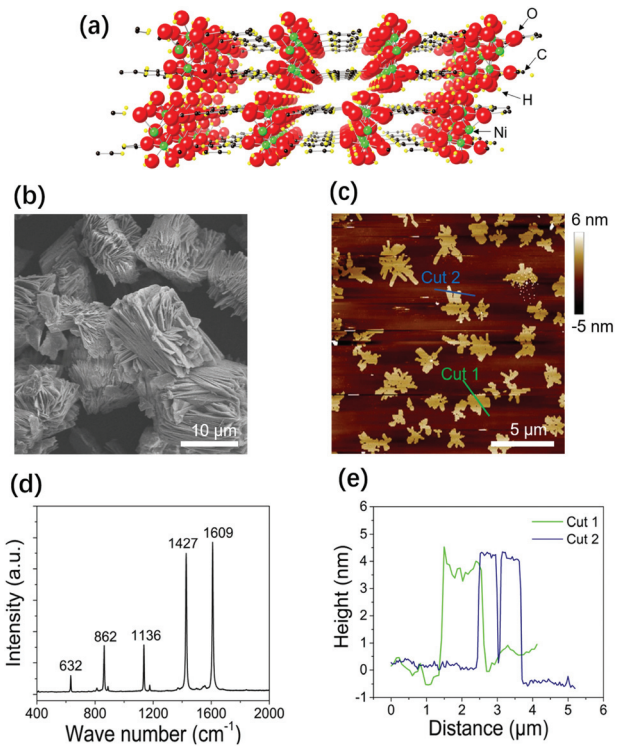

Fig. 1 (a) Schematic diagram of the 2D Ni-MOF crystal structure. (b) SEM image of the Ni-MOF showing a 2D layer structure. (c) AFM image of the Ni-MOF dissolved in an IPA solution. (d) Raman spectrum of the Ni-MOF under the excitation of a 532 nm laser. (e) The thickness of the cut lines shown in (c).

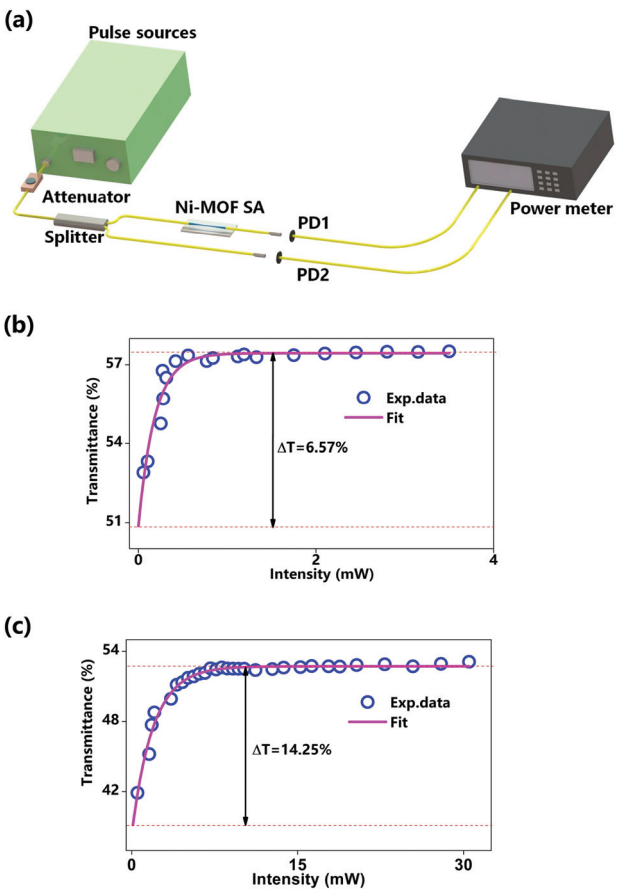

Fig. 2 (a) The setup of balanced twin-detector measurement. (b) The measured saturable absorption data and their corresponding fitting curve under 1564 nm and (c) 1934 nm laser irradiation.

an evanescent field, we adsorbed the material on the microfiber surface. Real-time observation of fiber loss changes helps to control the depth of deposition. The power loss is about 3 dB after deposition in this work.

The saturable absorption of the Ni-MOF is determined by balanced synchronous twin-detector measurement [Fig. 2(a)]. The saturable absorption data is obtained based on the same microfiber Ni-MOF SA and their corresponding fitting curve is measured under two different wavelength laser sources. A self-made laser which can generate 728 fs pulse duration at 1564 nm is used as one of the laser sources. We used an adjustable attenuator and a 50 : 50 fiber-pigtailed optical output coupler; this can detect the reference signal and absorption at the same time. In the same way, we used an ultrashort pulse fiber laser as the other laser source (1.2 ps pulse duration, 1934 nm wavelength and 13.3 MHz pulse repetition frequency). The transmitted power as a function of the incident optical power for the Ni-MOF SA was recorded by continuous adjustment of the attenuator and the transmittance of the Ni-MOF SA tends to be constant with increasing peak intensity. We can clearly see the nonlinear transmission curve of the Ni-MOF SA. The experimental data can be fitted with the following formula:

$$T(I) = 1 - \Delta T \exp(-I/I_{sat}) - T_{ns} \quad (1)$$

where $T(I)$ is the transmission, ΔT is the modulation depth, I is the input intensity, I_{sat} is the saturation power intensity, and T_{ns} is the non-saturated loss. We used the same microfiber, and these are shown in Fig. 2(b) and (c). We obtained the corresponding saturable absorption parameters. Nonlinear optical absorption of the Ni-MOF SA was characterized, and the modulation depths were found to be 6.57% and 14.25% with 0.15 mW and 1.923 mW saturation intensity under 1564 nm and 1934 nm laser irradiation, respectively. The nonlinear absorption properties of the Ni-MOF indicate that it can be used as a SA for ultrashort fiber lasers.

3. Experimental setup

To study the wideband saturable absorption of the Ni-MOF for ultrashort pulse generation, a microfiber-based Ni-MOF SA is

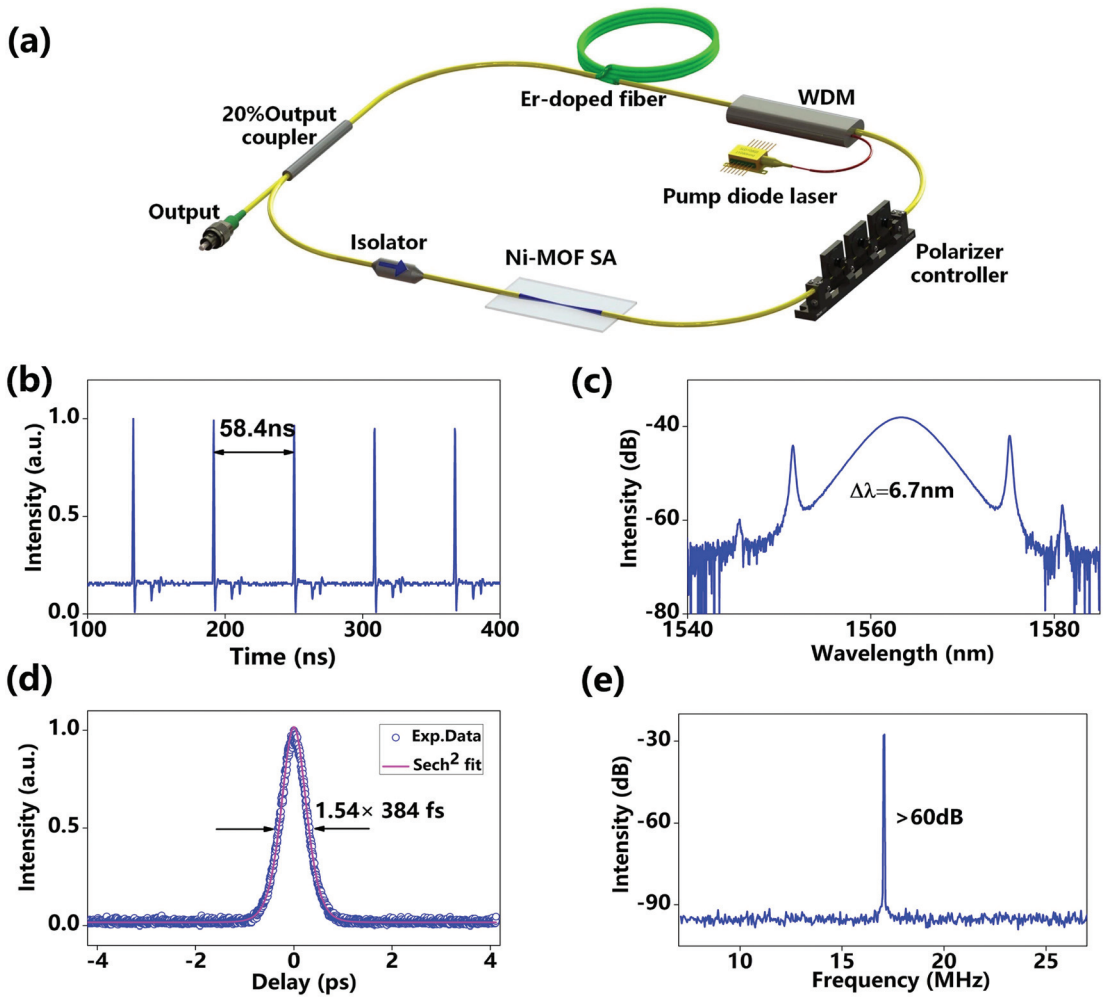

Fig. 3 Er:fiber mode-locked laser: (a) schematic of the cavity; (b) oscilloscope trace; (c) optical spectrum; (d) autocorrelation trace; and (e) fundamental radiofrequency spectrum.

used in Er- and Tm-doped fiber lasers, respectively. For each laser cavity, a typical all-fiber-integrated ring cavity configuration is adopted, including the fiber amplifier [Fig. 3(a) and 4(a)], optical output coupler, polarization independent inline fiber isolator and polarization controller. The Er amplifiers have a 4.5 m long EDF and are pumped by 980 nm laser diodes. The total length of the erbium (Er)-doped fiber laser cavity is 11.72 m and the net cavity dispersion is calculated to be −0.126 ps^2. The Tm amplifiers consist of a 2.4 m long Tm fiber (Nufern SM-TSF-9/125), pumped by a continuous wave 1570 nm fiber laser. The total length of the Tm fiber-based cavity is about 14.4 m. The net cavity dispersion is about −1.012 ps^2.

4. Results and discussion

4.1 Mode-locked Er:fiber laser characterization

The Ni-MOF-based mode-locking operation self-started when the pump power was increased to 34.6 mW. The cavity round-trip time is 58.4 ns, which is in accord with the 11.72 length of the cavity [Fig. 3(b)], with an output power of 106 μW. The spectrum is centered at 1563 nm and the 3 dB bandwidth is about 6.7 nm [Fig. 3(c)]. The pulse duration is 384 fs, a good fit with a $sech^2$ pulse shape [Fig. 3(d)]. The time-bandwidth product (TBP) is estimated to be 0.318, indicating that the generated pulses are slightly chirped. The fundamental radiofrequency (RF) spectrum of the generated pulses is about 17 MHz with a signal-to-noise ratio of >64 dB [Fig. 3(e)].

4.2 Mode-locked Tm:fiber laser characterization

The mode-locking operation was observed at a pump power of 365 mW with an output power of 2.87 mW. The interval time of the laser pulses is 72.2 ns. It generates a stable train of pulses and the pulse characteristics are shown in Fig. 4(b). Fig. 4(c) shows the spectrum which is centered at 1882 nm with a 3 dB bandwidth of about 3.5 nm. The pulse duration is 1.3 ps [Fig. 4(d)], resulting in a TBP of 0.39. The fundamental radiofrequency spectrum is 13.9 MHz, which is shown in Fig. 4(e) without any anharmonic components, indicating that our laser has a relatively low supermode noise.

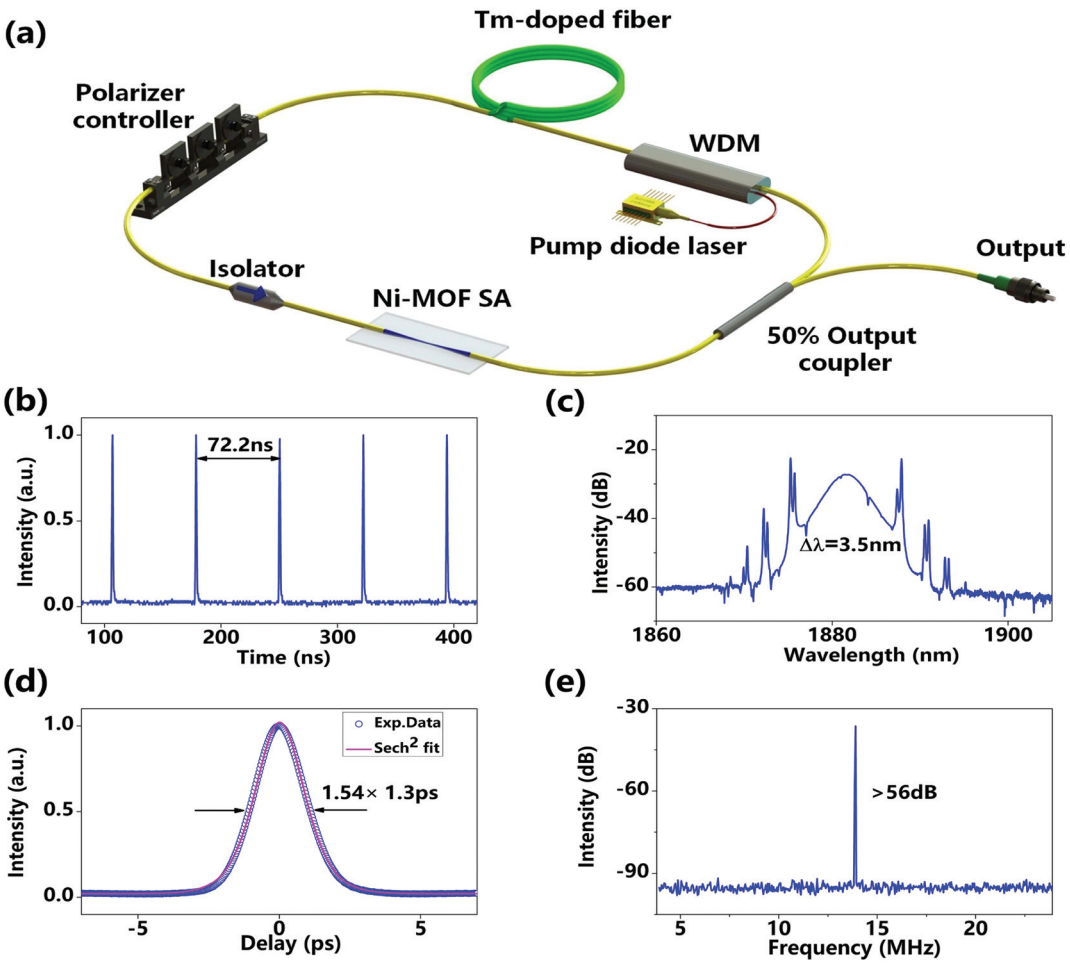

Fig. 4 Tm:fiber mode-locked laser: (a) schematic of the cavity; (b) oscilloscope trace; (c) optical spectrum; (d) autocorrelation trace; and (e) fundamental radiofrequency spectrum.

5. Conclusions

In this paper, we have reported the fabrication of a microfiber-based MOF by an optical deposition process. For the first time, we have demonstrated that the Ni-MOF can generate broadband ultrashort pulses by mode-locking. We developed Er- and Tm-doped fiber lasers, operating at 1563 nm and 1882 nm with pulse durations of 385 fs and 1.3 ps, respectively. Nonlinear optical absorption of the MOF SA was characterized and the modulation depths were found to be 6.57% and 14.25% with 0.15 mW and 1.923 mW saturation power under 1564 nm and 1934 nm laser irradiation, respectively. Our results highlight the potential of such a nanomaterial with exceptional optical properties and remarkable opportunities for future SA technologies.

Conflicts of interest

There are no conflicts to declare.

Acknowledgements

The work presented in this article is partially supported by the National Natural Science Foundation of China (NSFC) (51778030, 51978024). X. J. acknowledges the support from the National Natural Science Foundation of China (61805146).

References

1 F. Bonaccorso, Z. Sun, T. Hasan and A. C. Ferrari, *Nat. Photonics*, 2010, **4**, 611–622.
2 F. Xia, T. Mueller, Y.-m. Lin, A. Valdes-Garcia and P. Avouris, *Nat. Nanotechnol.*, 2009, **4**, 839–843.
3 M. Liu, X. Yin, E. Ulin-Avila, B. Geng, T. Zentgraf, L. Ju, F. Wang and X. Zhang, *Nature*, 2011, **474**, 64–67.
4 A. Martinez and Z. Sun, *Nat. Photonics*, 2013, **7**, 842–845.
5 K. S. Novoselov, V. I. Fal'ko, L. Colombo, P. R. Gellert, M. G. Schwab and K. Kim, *Nature*, 2012, **490**, 192–200.
6 R. I. Woodward and E. J. R. Kelleher, *Appl. Sci.*, 2015, **5**, 1440–1456.
7 V. Tran, R. Soklaski, Y. Liang and L. Yang, *Phys. Rev. B: Condens. Matter Mater. Phys.*, 2014, **89**, 235319.
8 M. Zhang, R. C. T. Howe, R. I. Woodward, E. J. R. Kelleher, F. Torrisi, G. Hu, S. V. Popov, J. R. Taylor and T. Hasan, *Nano Res.*, 2015, **8**, 1522–1534.
9 G. Hu, T. Albrow-Owen, X. Jin, A. Ali, Y. Hu, R. C. T. Howe, K. Shehzad, Z. Yang, X. Zhu, R. I. Woodward, T.-C. Wu, H. Jussila, J.-B. Wu, P. Peng, P.-H. Tan, Z. Sun, E. J. R. Kelleher, M. Zhang, Y. Xu and T. Hasan, *Nat. Commun.*, 2017, **8**, 278.
10 Y.-W. Song, S.-Y. Jang, W.-S. Han and M.-K. Bae, *Appl. Phys. Lett.*, 2010, **96**, 051122.
11 D. Mao, S. Zhang, Y. Wang, X. Gan, W. Zhang, T. Mei, Y. Wang, Y. Wang, H. Zeng and J. Zhao, *Opt. Express*, 2015, **23**, 27509–27519.
12 M. Zhang, G. Hu, G. Hu, R. C. T. Howe, L. Chen, Z. Zheng and T. Hasan, *Sci. Rep.*, 2015, **5**, 17482.
13 Y. Ge, Z. Zhu, Y. Xu, Y. Chen, S. Chen, Z. Liang, Y. Song, Y. Zou, H. Zeng, S. Xu, H. Zhang and D. Fan, *Adv. Opt. Mater.*, 2018, **6**, 1701166.
14 A. Favron, E. Gaufrès, F. Fossard, A.-L. Phaneuf-L'Heureux, N. Y. W. Tang, P. L. Lévesque, A. Loiseau, R. Leonelli, S. Francoeur and R. Martel, *Nat. Mater.*, 2015, **14**, 826–832.
15 M. Zhang, Q. Wu, F. Zhang, L. L. Chen, X. X. Jin, Y. W. Hu, Z. Zheng and H. Zhang, *Adv. Opt. Mater.*, 2019, **7**, 1800224.
16 O. M. Yaghi, M. O'Keeffe, N. W. Ockwig, H. K. Chae, M. Eddaoudi and J. Kim, *Nature*, 2003, **423**, 705–714.
17 X. T. Jiang, L. J. Zhang, S. X. Liu, Y. Y. Zhang, Z. L. He, W. J. Li, F. Zhang, Y. H. Shi, W. Lu, Y. Li, Q. Wen, J. G. Li, J. Feng, S. C. Ruan, Y. J. Zeng, X. Zhu, Y. R. Lu and H. Zhang, *Adv. Opt. Mater.*, 2018, **6**, 1800561.
18 C. Gu, H. Zhang, P. X. You, Q. Zhang, G. Q. Luo, Q. Shen, Z. B. Wang and J. B. Hu, *Nano Lett.*, 2019, **19**, 9095–9101.
19 M. Lismont, L. Dreesen and S. Wuttke, *Adv. Funct. Mater.*, 2017, **27**, 1606314.
20 D. Maspoch, D. Ruiz-Molina, K. Wurst, N. Domingo, M. Cavallini, F. Biscarini, J. Tejada, C. Rovira and J. Veciana, *Nat. Mater.*, 2003, **2**, 190–195.
21 H. S. Cho, H. Deng, K. Miyasaka, Z. Dong, M. Cho, A. V. Neimark, J. K. Kang, O. M. Yaghi and O. Terasaki, *Nature*, 2015, **527**, 503–507.
22 F. Qu, H. Jiang and M. Yang, *Nanoscale*, 2016, **8**, 16349–16356.
23 O. R. Evans and W. B. Lin, *Acc. Chem. Res.*, 2002, **35**, 511–522.
24 D. D. Wang, J. J. Zhou, R. H. Chen, R. H. Shi, G. L. Xia, S. Zhou, Z. B. Liu, N. Q. Zhang, H. B. Wang, Z. Guo and Q. W. Chen, *Biomaterials*, 2016, **107**, 88–101.
25 N. Stock and S. Biswas, *Chem. Rev.*, 2012, **112**, 933–969.
26 Y. Jiao, G. Chen, D. Chen, J. Pei and Y. Hu, *J. Mater. Chem. A*, 2017, **5**, 23744–23752.
27 S. Bordiga, C. Lamberti, G. Ricchiardi, L. Regli, F. Bonino, A. Damin, K. P. Lillerud, M. Bjorgen and A. Zecchina, *Chem. Commun.*, 2004, 2300–2301.
28 S. He, Z. Li, J. Wang, P. Wen, J. Gao, L. Ma, Z. Yang and S. Yang, *RSC Adv.*, 2016, **6**, 49478–49486.
29 Y. W. Song, K. Morimune, S. Y. Set and S. Yamashita, *Appl. Phys. Lett.*, 2007, **90**, 1173.

